

## Macrostructural Biofilm Characterization via Textural Image Analysis by SGLDM and GLRLM

Marie-Noëlle Pons\*, K. Milferstedt,\*\*  
E. Morgenroth\*\*,\*\*\*

\*Laboratoire des Sciences du Génie Chimique CNRS, Nancy University, BP 20451  
54001 Nancy cedex, France (e-mail: Marie-Noelle.Pons@ensic.inpl-nancy.fr)

\*\*Dept Civil & Env. Eng., University of Illinois at Urbana Champaign, 205 North Mathews Av., MC250,  
Urbana, IL 61801, USA (milferst@uiuc.edu, emorgenr@uiuc.edu)

\*\*\* Dept. Animal Sciences, University of Illinois at Urbana-Champaign,

---

**Abstract:** The macrostructure development of biofilms grown in an annular reactor and in a rotating biological contactor has been monitored using the Spatial Gray-level Dependence Method (SGLDM) and the Gray-Level Run Length Method (GLRLM). Due to the large number of descriptors, Principal Components Analysis was used to sort the results. Both methods look promising for biofilm monitoring.

---

### 1. INTRODUCTION

Biofilms are ubiquitous forms of ecosystem development combining different types of microorganisms (bacteria, fungi, algae, protozoa, etc.) They can be useful as in wastewater treatment systems where many biofilm applications are found (Hansford et al., 1978; Najafpour et al., 2005; Nilsson et al., 2006 among many others). But they can also endanger human health (Ebrey et al., 2004; Kipnis et al., 2006).

Generally speaking, biofilms develop on a supporting media. The chemical and physical stresses they undergo contribute to limit their expansion. In the case of rotating biological contactors (RBC), biomass is fixed on a circular or cylindrical support which rotates slowly around its axis. In its basic configuration the support undergoes periodic exposition to air and wastewater. The biofilm excess is stripped off by shear forces exerted during its passage in water. Proper application of shear forces is a way to control biomass development.

Several indirect methods have been proposed to monitor biomass development in biofilms. Optical methods combined with image analysis are interesting as, with a proper experimental setup, they can be used to monitor biofilm over extended period of time, with little disturbance of the ecosystem. Milferstedt et al. (2006) have developed such a scanner-based procedure and have used it to estimate the biofilm total solids content and thickness. Depending upon the optical resolution method, structural information can also be collected. This information is provided indirectly by the visual textural parameters that can be extracted from images. Binarization (i.e. segmentation between regions "with biomass" and regions "without biomass") is often required (Yang et al., 2000). Another approach consists in working directly on the gray-level images. This could be particularly useful for low resolution images used to examine large biofilm areas.

Many texture analysis algorithms have been reported in literature: Spatial Grey Level Dependence Method (SGLDM) (Haralick et al., 1973), Grey Level Run Length Method (GLRLM) (Galloway, 1975), Gray Level Difference Method (Wezaska et al., 1976) or Power Spectral Method (PSM) (Lendaris and Stanley, 1970). It is often difficult to select the most appropriate method. Some advocate SGLDM (Conners and Harlow, 1980) when for others (Tang, 1998) GLRLM are more appropriate.

In a previous work, Milferstedt et al. (2007) has successfully used SGLDM to monitor the macrostructure of biofilm developed on flat slides in an annular reactor and visualized with a desktop scanner. In the present contribution, GLRLM is compared with SGLDM on two types of biofilm images: biofilm developed in an annular reactor on flat rectangular slides and visualized with a stereomicroscope and biofilm developed in a lab-scale RBC and visualized with a desktop scanner

### 2. EXPERIMENTAL METHODS

#### 2.1. Annular reactor

The experimental setup is given in Fig. 1. The reactor (model 1120, BioSurface Technologies Corp., Bozemann, MT) was operated at different rotation speeds (300 rpm or 385 rpm) with a hydraulic retention time of 23 min. The inner drum was fitted with 20 polycarbonate removable slides. The reactor was fed with autoclaved synthetic medium (glucose-based with mineral salts) as described by Milferstedt et al. (2006).

Biofilm images were regularly acquired with a Zeiss Stemi 2000c stereo microscope (Carl Zeiss, Jena, Germany) equipped with a Nikon Coolpix 4500 digital camera (Nikon Inc.). A 2272 x 1704 pixels image (1 pixel = 2.4  $\mu\text{m}$  x 2.4  $\mu\text{m}$ ) represents a 22.4 mm<sup>2</sup> biofilm surface.

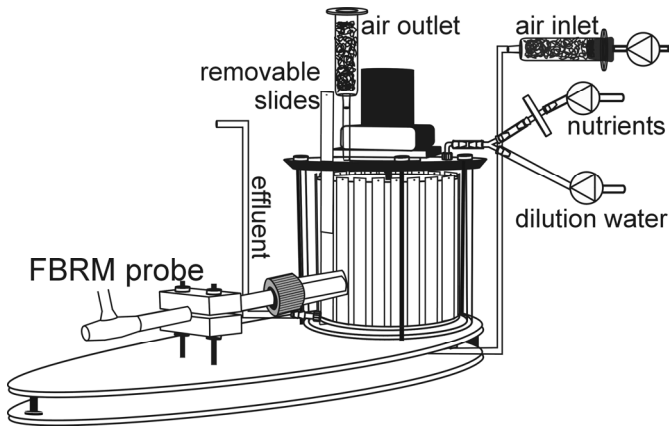


Fig. 1. The annular reactor

### 2.2. Rotating biological contactor

The in-house rotating biological contactor is made out of Plexiglass (Fig.2.). The disks (diameter = 100 mm) were rotating at 4 rpm. The reactor, of volume 2 liters, was fed with raw wastewater collected after the grit removal in a local wastewater treatment plant for 35 days. The feed was then switched to a synthetic complex media based on meat extract, sugar, ammonium sulphate and phosphoric acid. Up to 4 disks (spacing = 10 mm) can be placed on the rotation axis. Disk 1 was run from day 0 to day 55, disk 2 from day 1 to 34, disk 3 from day 21 to 55 and disk 4 from day 35 to 55. The hydraulic residence time was 20 hrs. Images (3364 x 3624 pixels) of the disks are regularly captured with a desktop scanner (Epson PERF4490P) at a resolution of 800 dpi (1 pixel = 31.8  $\mu\text{m}$  x 31.8  $\mu\text{m}$ ).

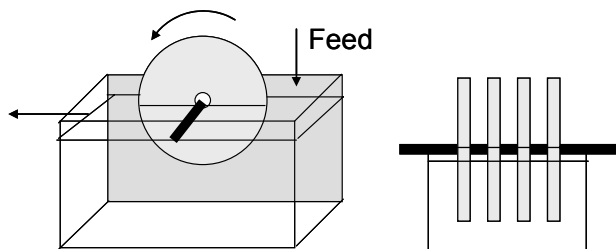


Fig. 2. Rotating biological contactor: Side view (right) and perspective view (left)

### 3. IMAGES

Test images were extracted from the Vistex data base (MIT Media Laboratory, USA) (Fig.3.). Images (Fig. 4 to 6) textures were also created using sinusoidal functions with Scilab (INRIA, Rocquencourt, France) to give circular ("C"), radial ("R" and radio-circular ("RC") textures.

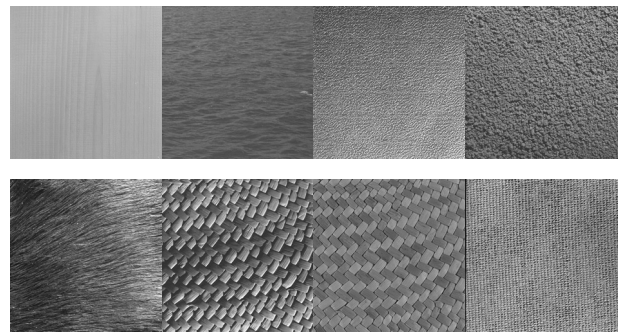


Fig.3. Vistex textures: Wood.0002, Water.0006, Metal.0001, Food.0005 (first row, left right), Fabric.0005, Fabric.0003, Fabric.0000, Fabric.0017 (second row, left to right).

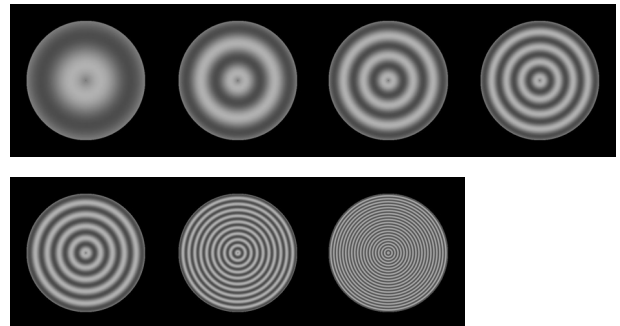


Fig. 4. "C" textures

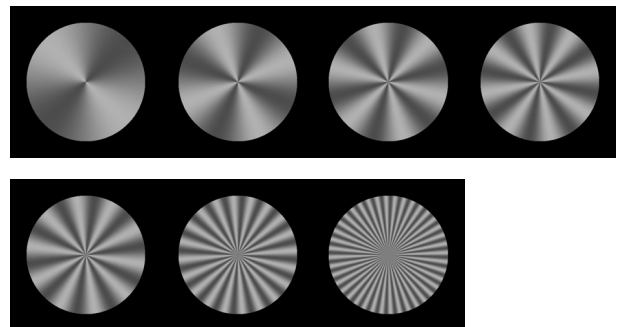


Fig. 5. "R" textures

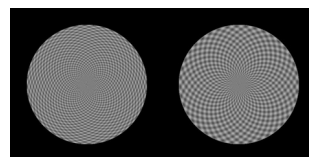


Fig. 6. "RC" textures

Figure 7 shows the location of the images on a rotating annular reactor slide. Figures 8 and 9 present images of slide 14 collected on day 9 (Fig. 8.) and on day 71 (Fig. 9) (end of the experiment). On the first series hairy biomass is observed on the surface of the biofilm. It has largely disappeared at the end of the experiment.

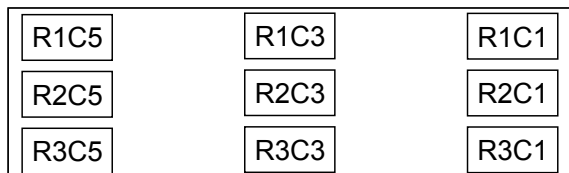


Fig. 7. Localization of the images on the slide (annular reactor)

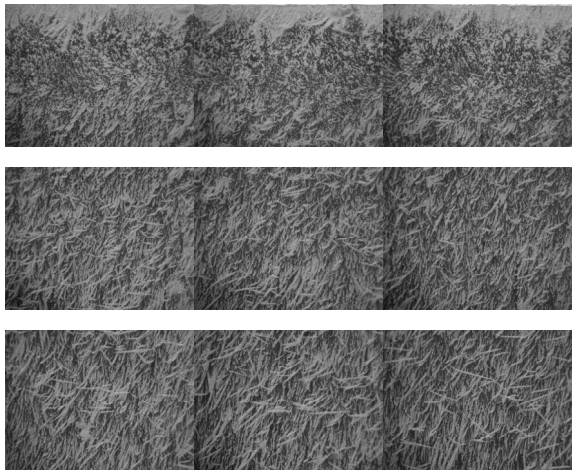


Fig. 8. RiCj series of images for slide 14 on day 9

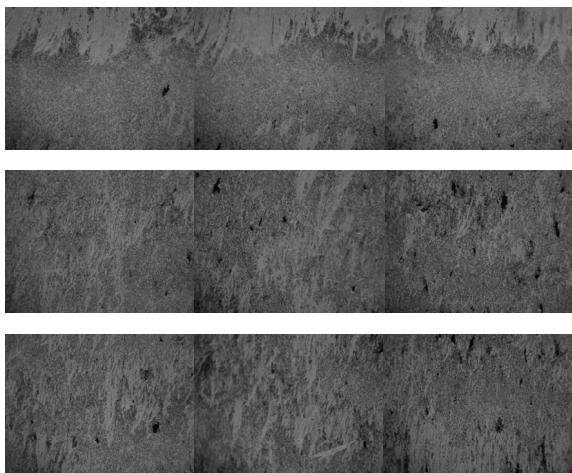


Fig.9. RiCj series of images for slide 14 on day 71

Figure 10 presents some of the images collected on disk 1 between the beginning and the end of the experiment. The biofilm develops until homogenous and thick coverage of the disk is reached. Then voids start to appear and gradually large fragments of biofilm are stripped off.

#### 4. TEXTURE CHARACTERIZATION

The spatial grey level dependence method is based on a set of probability density functions:  $f(i, j|d, \theta)$  is the probability of having a pair of pixels of gray levels  $i$  and  $j$ , with an interspacing  $d$  and a direction  $\theta$  between the pixels. Usually descriptors of the SGLDM matrix are used to compare textures. Haralick et al. (1973) have proposed a number of them, such as Energy, Entropy, Correlation, Local Homogeneity, Inertia, etc.

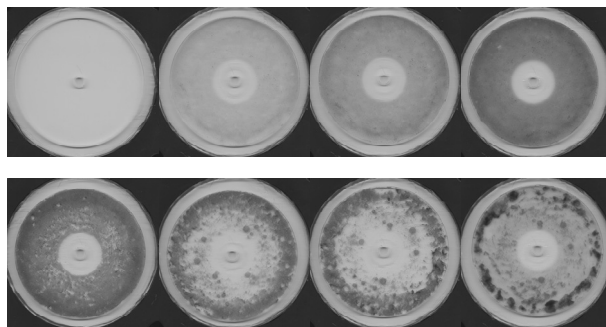


Fig. 10. Image of disk 1 after, on first row, 0,14, 20, 27 days and on second row, 35, 39, 41 and 52 days

In the Gray Level Run Length Method (GLRLM) the number of gray level runs, i.e. of set of adjacent pixels having the same gray levels, of various lengths are computed. Galloway (1975) has originally proposed five features (Short Run Emphasis (SRE), Long Run Emphasis (LRE), Gray-Level Nonuniformity (GLN), Run Length Nonuniformity (RLNp and Run Percentage (RP)) to describe the GLRLM matrix. Chu et al. (1990) have added two descriptors: Low Gray-Level Run Emphasis (LGRE), High Gray-Level Run Emphasis (HGRE). Finally four more descriptors have been proposed by Dasarathy and Holder (1991): Short Run Low Gray-Level Emphasis (SRLGE), Short Run High Gray-Level Emphasis (SRHGE), Long Run Low Gray-Level Emphasis (LRLGE) and Long Run High Gray-Level Emphasis (LRHGE).

Obviously, if SGLDM and GLRLM can be applied directly to the images acquired from the annular reactor, it is not the case for the images acquired from the disks. A geometrical transformation was therefore applied in order to obtain rectangular images compatible with the texture characterization methods. The principle is schematized in Fig. 11. On the new images, the radii are expanded along lines. The transformation is done by a Visual Basic macro embedded in Visilog 6.5 (Noesis, Les Ulis, France). For these images, SGLDM and GLRLM are run on an area of interest which corresponds to the circular zone between 35% and 98% of the disk radius. The SGLDM and GLRLM algorithms were implemented as FORTRAN codes.

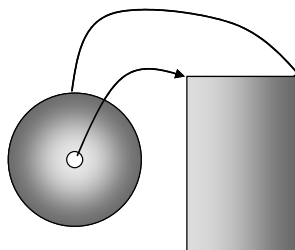


Fig. 11. Transformation of a disk image into a rectangular image where the x-axis is the radius and the y-axis the angular position.

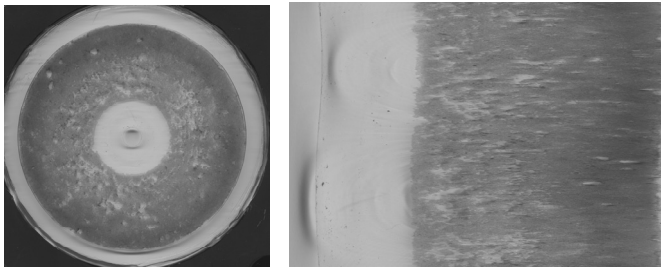


Fig. 12. Disk 1 on day 35 and its transformed image.

## 5. RESULTS

### 5.1 Test images

Due to the number of available descriptors available with each method, it is often difficult to get a clear view just by listing the values. Furthermore there is often a large degree of correlation between the descriptors. Data classification and analysis has been performed by Principal Components Analysis (Scilab, INRIA, Rocquencourt).

SGLDM and GLRLM were first applied to the Vistex test images, which have been selected for their apparent similarity with the biofilm images obtained with the annular reactor. Two directions were used ( $0^\circ$  and  $90^\circ$ ) and the sets of descriptors obtained with both directions were combined for data classification. For SGLDM it is necessary to select a distance. A distance of 10 pixels, which represents  $\approx 2\%$  of the image size, has been selected. Table 1 gives the number of principal components to be retained depending upon the total variability explained.

GLRLMsel refers to the following set of descriptors: SRLGE, SRHGE, LRLGE, LRHGE. SGLDMsel refers to the following set of SGLDM descriptors: Energy (ENG), Contrast (CON), Correlation (COR), Homogeneity (HOM), Textural Entropy (TE) and Inertia (IN) (Haralick et al., 1973).

Table 1. Fraction of variability explained with respect to the number of principal components retained for different set of descriptors applied to the Vistex test images.

Nb of PCs	GLRLMall	GLRLMsel	SGLDMsel
1	0.61	0.73	0.64
2	0.77	0.93	0.88
3	0.90	0.99	0.94

Figure 13 compared the distributions with respect to the two first principal components of the Vistex textures for SGLDM and GLRLM using the selected sets of descriptors. In the SGLDM plot the data points representing the different textures are well distributed. With GLRLM, the data points are surprisingly aligned, except for one point which corresponds to Fabric.005.

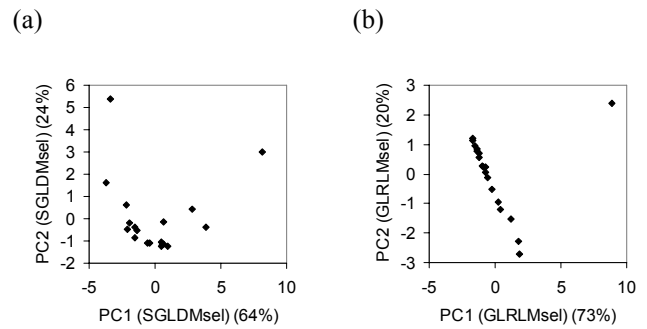


Fig. 13. Comparison of SGLDMsel (a) and GLRLMsel (b)

A similar exercise was conducted for the textures “C”, “R” and “RC” (Fig. 14). A distance of 50 pixels ( $\approx 5\%$  of the image size) was chosen. Features at  $0^\circ$  and  $90^\circ$  were combined as previously. The textures are well separated by SGLDMsel. For GLRLMsel the alignment observed on the Vistex textures for the representation in the PC1-PC2 plane is visible but a better separation is obtained in the PC1-PC3 plane.

Table 3. Fraction of variability explained with respect to the number of principal components retained for different set of descriptors applied to the Vistex test images.

Nb of PCs	GLRLMall	GLRLMsel	SGLDMsel
1	0.61	0.73	0.41
2	0.77	0.93	0.78
3	0.90	0.99	0.93

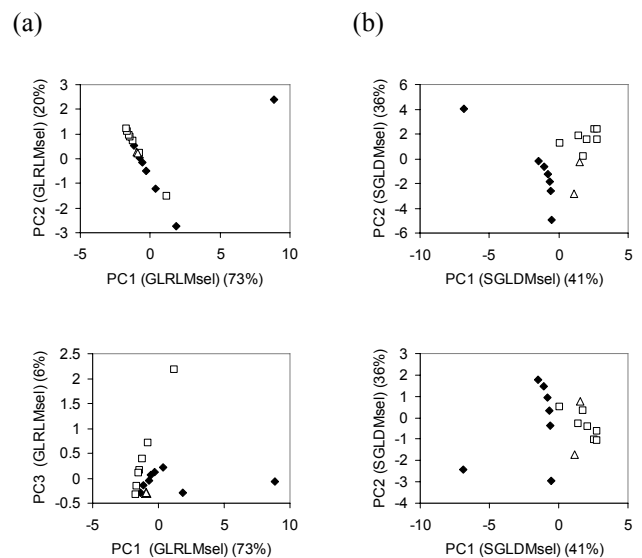


Fig.14. Comparison of the classification of “C” (◆), “R” (□) and “RC” (△) textures by GLRLMsel (a) and SGLDMsel (b)

### 5.2 Annular reactor biofilm

For the total set of 151 images taken on slide 14 of the annular reactor over 72 days, 73% and 14% of the variability can be explained by the two first principal components and SGLDMsel. 90% and 6% can be explained by the two first principal components for GLRLMsel. The inter-pixel distance was 120  $\mu\text{m}$  (50 pixels) for SGLDMsel. Features at 0° and 90° were combined as previously

The mean values were computed using the five sets of images available along each row (Fig. 15). With both methods a difference in the texture is seen between row 1 (which contains a large amount of microbial filaments, probably fungi) and row 2 and 3, which have a similar behaviour. This difference is less obvious after the second speed increase. The GLRLMsel method detects a change in texture shortly after each stress application. With the SGLDMsel method, a gradual change of the texture is observed, except for Row 1. Both methods indicate that the texture is homogenous along row, with small dispersion.

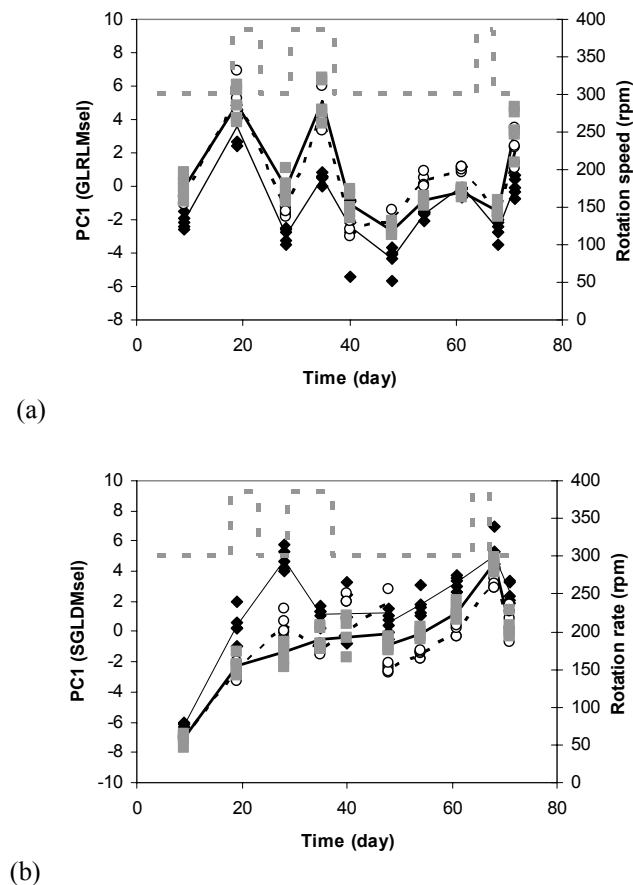


Fig. 15. Evolution of the biofilm texture according to the first principal component by GLRLMsel (a) and SGLDMsel (b) for the annular reactor experiment. ( $\blacklozenge$ ) row 1, ( $\circ$ ) row 2, ( $\blacksquare$ ), row 3, thin dark line = mean for row 1, dotted dark line = mean row 2, thick dark line = mean row 3, dotted grey line = rotation speed.

### 5.3 Biological rotating contactor

For the total set of 77 images taken on the four disks of the biological rotating contactor over 55 days, 66% and 18% of the variability can be explained by the two first principal components for SGLDMsel. 87% and 12% can be explained by the two first principal components for GLRLMsel. The inter-pixel distance was 4.8 mm (50 pixels) in the 0° direction (corresponding to the radial direction in the original image) and 2.5° in the 90° direction (corresponding to the angular direction in the original image). The methods were applied to the zone effectively occupied by the biofilm (i.e. the centre part was discarded..

In Fig. 16, the variations in the texture have been monitored by GLRLMsel. Disks 1 and 2 developed similarly during the first 35 days. The stress applied to disk 1 by changing the feed composition induces a sharp change in the texture, which is not seen on disk 3, on which the biofilm is younger. The parallel textural development of the disks is best visualized by considering the time spent in the reactor as shown in Fig. 17 for SGLDMsel.

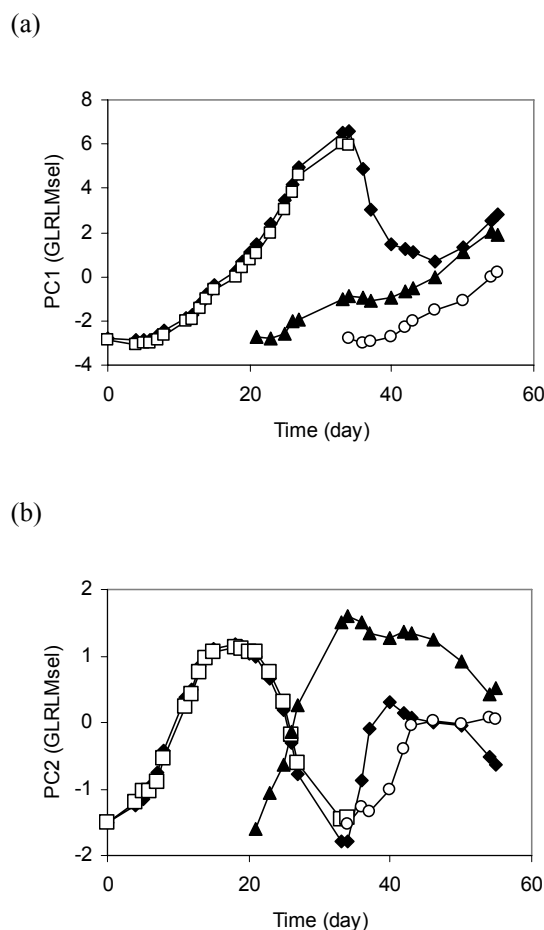
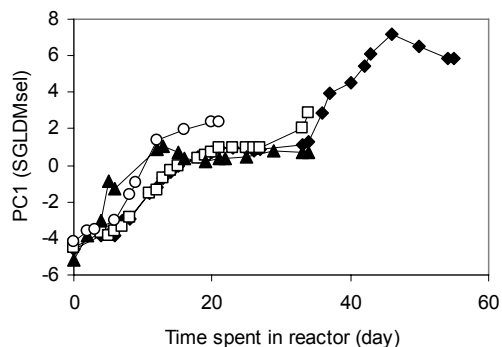
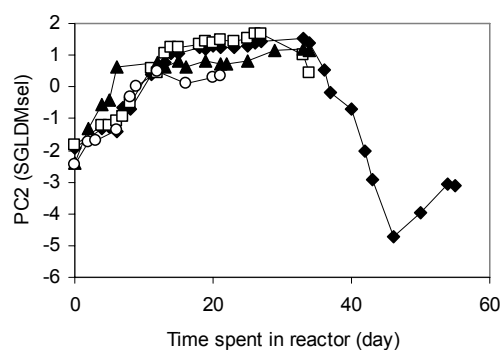


Fig. 16. Evolution of the biofilm texture according to the first (a) and second (b) principal components by GLRLMsel, ( $\blacklozenge$ ) disk 1, ( $\square$ ) disk 2, ( $\blacktriangle$ ) disk 3, ( $\circ$ ) disk 4.



(a)



(b)

Fig. 18. Superposition of the evolution of the biofilm texture according to the first (a) and second (b) principal components by SGLDMsel, starting from the initial time in the reactor . (♦) disk 1, (□) disk 2, (▲) disk 3, (○) disk 4.

## 6. CONCLUSIONS

SGLDM and GLRLM were used with reduced number of descriptors to monitor the development of two different types of biofilm. Principal Components Analysis was necessary to analyze the results due to the large number of data. Two principal components were sufficient for the biofilm images. Changes of texture related to physical stress (annular reactor case) or chemical stress (rotating biological reactor) could be observed. Due to the similar performance, no clear choice of one of the methods could be done. However it should be underlined that SGLDM requires the choice of an appropriate inter-pixel distance, which is not the case for GLRLM.

## 7. ACKNOWLEDGEMENTS

The authors are thankful for financial support in part from the CNRS/UIUC cooperation program, a CAREER award to Eberhard Morgenroth from the National Science Foundation under grant No. BES-0134104 and to The WaterCAMPWS, a Science and Technology Center of Advanced Materials for the Purification of Water with Systems under the National Science Foundation agreement number CTS-0120978.

## REFERENCES

- Chu A., C.M. Sehgal and J.F. Greenleaf (1990) Use of gray value distribution of run lengths for texture analysis. *IEEE Trans. Image Processing*, **2**, 429-441.
- Conners, R.W. and C.A. Harlow (1980) A theoretical comparison of texture algorithms. *IEEE Trans. Patt. Anal. Mach. Intelligence*, **PAMI-2**, 204-222
- Dasarathy, B.R. and E.B. Holder (1991) Image characterization based on joint gray-level run-length distributions, *Pattern Recognition Letters*, **12**, 497-502.
- Ebrey, R., M.S. Hamilton, G. Cairns and H.M. Lappin-Scott (2004) Biofilms and hospital-acquired infections. In: *Microbial biofilms* (Ghanoum M, O'Toole G.A., eds) 294-313, Washington, DC; ASM Press.
- Galloway, M.M. (1975) Texture analysis using gray level run lengths. *Comput. Graphics Image Process.* **4**, 172-179.
- Hansford, G.S., J.F. Andrews, C.G. Grieves and A.D. Carr (1978) A steady-state model for the rotating biological disc reactor. *Water Research*, **12**, 855-868.
- Haralik R.M., K.S. Shanmugan and I. Dinstein (1973) Textural features for image classification. *IEEE Trans. Syst. Man, Cybern.* **SMC-3**, 610-621.
- Kipnis, E., T. Sawa and J. Wiener-Kronish (2006) Targeting mechanisms of *Pseudomonas aeruginosa* pathogenesis. *Med. Mal. Infect.* **36**, 78-91.
- Lendaris G.O. and G.L. Stanley (1970) Diffraction pattern sampling for automatic pattern recognition, *Proc. IEEE*, **58**, 198-216.
- Milferstedt, K., M.N. Pons M.N. and E. Morgenroth (2006) Optical method for long-term and large-scale monitoring of spatial biofilm development. *Biotechnology and Bioengineering*, **94**, 773-782.
- Milferstedt, K., M.N. Pons M.N. and E. Morgenroth (2007) texture analysis of spatial biofilm development. *Water Science and Technology*, **55**(8-9), 481-488.
- Najafpour, G., H.A. Yieng, H. Younesi and A. Zinatizadeh (2005) Effect of organic loading on performance of rotating biological contactors using palm oil mill effluents. *Process Biochemistry*, **40**, 2879-2884
- Nilsson, I., A. Möller, B. Mattiasson, M.S.T. Rubindamayugi and U. Welander (2006) Decolorization of synthetic and real textile wastewater by the use of white-rot fungi. *Enzyme and Microbial Technology*, **38**, 94-100.
- Tang X. (1998) Texture information in run-length matrices. *IEEE Transactions on Image Processing*, **7**, 1602-1609.
- Weska J.S., C.R. Dyer and A. Rosenfeld (1976) A comparative study of texture measures for terrain classification. *IEEE Trans. Syst. Man, Cybern.* **SMC-6**, 269-285.
- Yang X.M., H. Beyenal, G. Harkin and Z. Lewandowski (2000) Quantifying biofilm structure using image analysis. *J. Microbiol. Methods*. **39**, 109-119.